



**A Lab-on-a-Chip system integrating tissue sample preparation and multiplex RT-qPCR for gene expression analysis in point-of-care hepatotoxicity assessment**

Journal:	<i>Lab on a Chip</i>
Manuscript ID:	LC-ART-07-2015-000798.R1
Article Type:	Paper
Date Submitted by the Author:	11-Aug-2015
Complete List of Authors:	Lim, Geok Soon; Nanyang Technological University, Chang, Joseph; Nanyang Technological University Singapore, Zhang, Lei; Nanyang Technological University, Electrical and Electronics Engineering Wu, R.G.; Singapore Institute of Manufacturing Technology, Wang, Zhiping; Singapore Institute of Manufacturing Technology, Cui, Kemi; Houston Methodist Research Institute, Wong, Stephen; Houston Methodist Research Institute,

**TITLE**

**A Lab-on-a-Chip system integrating tissue sample preparation and multiplex RT-qPCR for gene expression analysis in point-of-care hepatotoxicity assessment**

**AUTHORS**

1. **Geok Soon Lim**, Nanyang Technological University
2. **Joseph S. Chang**, Nanyang Technological University
3. **Zhang Lei**, Nanyang Technological University
4. **Ruige Wu**, Singapore Institute of Manufacturing Technology
5. **Zhiping Wang**, Singapore Institute of Manufacturing Technology
6. **Joseph S. Chang**, Nanyang Technological University
7. **Kemi Cui**, Houston Methodist Research Institute
8. **Stephen Wong**, Houston Methodist Research Institute, Weill Cornell Medical College of Cornell University

**CORRESPONDING AUTHOR**

Name: Lim Geok Soon

Contact: gslim1@e.ntu.edu.sg , [limgeoksoon@gmail.com](mailto:limgeoksoon@gmail.com)

Address: Block 765 Jurong West Street 74, Unit 15-05, Singapore 640765

**ABSTRACT**

A truly practical Lab-on-a-Chip (LOC) system for point-of-care testing (POCT) hepatotoxicity assessment necessitates the embodiment of full-automation, ease-of-use, and “sample-in-answer-out” diagnostic capabilities. To date, reported microfluidic devices for POCT hepatotoxicity assessment remain rudimentary as they largely only embody semi-quantitative or single sample/gene detection capabilities. In this paper, we describe, for the first time, an integrated LOC system that is somewhat close to a practical POCT hepatotoxicity assessment device – it embodies both tissue sample preparation and multiplex real-time RT-PCR. It features semi-automation, relatively easy-to-use, and “sample-in-answer-out” capabilities for multiplex gene expression analysis. Our tissue sample preparation module incorporating both a microhomogenizer and surface-treated paramagnetic microbeads yielded high purity mRNA extracts – considerably better than manual extraction means. A primer preloading surface treatment procedure and single-loading inlet on our multiplex real-time RT-PCR module simplifies off-chip handling procedures for ease-of-use. To demonstrate the efficacy of our LOC system for POCT hepatotoxicity assessment, we perform a preclinical animal study with the administration of cyclophosphamide, followed by

a gene expression analysis on two critical Liver Function Tests' protein biomarkers, aspartate transaminase (AST) and alanine transaminase (ALT). Our experimental results depict normalized fold changes of 1.62 and 1.31 for AST and ALT respectively, illustrating up-regulations in their expression levels and hence validating their selection as critical genes of interest. In short, we illustrate the feasibility of multiplex gene expression analysis in an integrated LOC system as a viable POCT means for hepatotoxicity assessment.

## 1. Introduction

Hepatotoxicity assessment traditionally involves two commonly used analytical methods: histopathology (such as microscopy and tissue study) and blood parameter analysis (otherwise known as Liver Function Tests). Both methods are generally accepted as the gold standard<sup>1</sup> by the medical community for liver assessment. Nevertheless, despite their acceptance, it is well known that they suffer from several shortcomings, particularly their inherent associated complexities which are largely incompatible with point-of-care testing (POCT). For example, the requirements of traditional hepatotoxicity assessment often involve trained personnel and multistep procedures; and complex logistics, including requiring multiple tools and equipment, and significant amount of processing/administrative time<sup>1-3</sup>. These shortcomings conflict with the basic requirements of POCT which is largely defined as “tests designed to be used at or near the site where the patient is located, that do not require permanent dedicated space, and that are performed outside the physical facilities of clinical laboratories”<sup>4</sup>.

To resolve the aforementioned intrinsic issues of traditional hepatotoxicity assessment, Lab-on-a-Chip (LOC) techniques may be employed to enable system miniaturization and procedural simplification. This would alleviate the aforesaid issues, including reduced reagents consumption, integration of several modules, the possibility of system automation and reduced process completion time<sup>5</sup>; thereby congruous to POCT. In particular, a truly practical LOC system for POCT hepatotoxicity assessment necessitates the embodiment of full-automation, ease-of-use, and “sample-in-answer-out” diagnostic capabilities.

Interestingly, the current art of microfluidics in hepatotoxicity studies largely embodies *in-vitro* liver drug metabolism and toxicity studies via cell/tissue culture maintained in biomimetic microenvironments<sup>6-8</sup>, and *in-situ* quantification of cellular fluorescence intensities to observe enzymatic reactions or expressions in toxicity-induced hepatocytes<sup>9</sup>. This present-day approach to microfluidic hepatotoxicity assessment is largely an adaptation of histopathology transposed onto LOC platforms. This is, hence, generally incompatible with POCT diagnostics or “on-the-spot” patient care because it requires time-consuming cell or tissue culture growth and the subsequent analysis.

Hitherto, there are several reported microfluidic nucleic acid testing (NAT) work<sup>5, 10-12</sup>, comprising a biomolecular diagnostic approach targeting different applications such as pathogen/disease detection and identification of environmental pollutants. Although these microfluidic NAT works have reportedly demonstrated their pertinence to POCT, their practical application in companion diagnostics and personalized healthcare are however limited. However, despite the rapid development of microfluidic devices in NAT work, reported POCT *ex-vivo* hepatotoxicity NAT-based devices in literature are exiguous, largely due to the following challenges: (i) the ability to perform sample preparation in terms of tissue handling and extraction of RNA in a microfluidic device; (ii) the ability to perform multiplex gene expression analysis; and (iii) the selection of target messenger RNAs (mRNAs) that are indicative of hepatotoxicity<sup>5, 13</sup>.

To address these challenges, in one recent study, Shaw *et al.*<sup>14</sup> developed a semi-quantitative microfluidic borosilicate glass chip featuring integrated RNA extraction and reverse-transcription polymerase chain reaction (RT-PCR) capable of interrogating up-regulations of CYP1A2 (derived from cytochrome P450) gene expression levels during hepatotoxicity. This particular microfluidic device, however, embodied only a single chambered

glass chip capable of a single gene expression analysis per experimental run, and a semi-quantitative methodology which required off-chip end-point analysis via capillary gel electrophoresis. Further, it required extensive off-chip sample preparation procedures (such as a liver tissue lysis), lacked multiplex gene expression analysis capability, and did not have an on-chip fully-quantitative (or real-time) detection methodology. Hence, although this microfluidic device is an important step towards a POCT for hepatotoxicity assessment, its application to a practical POCT is limited.

In this paper, we describe, for the first time, an integrated microfluidic NAT system that is closer to a practical POCT hepatotoxicity assessment device ever reported – it embodies both tissue sample preparation and multiplex real-time RT-PCR. Compared to the state-of-the-art, our microfluidic system features semi-automation, relatively easy-to-use, and “sample-in-answer-out” capabilities for multiplex gene expression analysis. Our tissue sample preparation module incorporates both a microhomogenizer and surface-treated paramagnetic microbeads<sup>15</sup> to perform on-chip tissue lysis and mRNA purification, allowing us to obtain high purity mRNA extracts – considerably better than manual extraction means. A primer preloading surface treatment procedure and single-loading assay inlet on our multiplex real-time RT-PCR module simplifies off-chip handling procedures, such as pre-mixing of different RT-PCR assays for multiple genes of interest (GOIs), for ease-of-use. Compared to previously reported designs in the literature for microfluidic POCT hepatotoxicity assessment, our proposed device is advantageous in terms of being able to directly interrogate a crude liver tissue sample, and investigate multiple gene targets in a single experimental run. Further, with an integrated fully-quantitative methodology, we are able to reduce post-amplification procedural steps and diagnostic time, thereby allowing for “sample-in-answer-out” diagnostic capability.

With regard to targeted mRNA sequences used to investigate hepatotoxicity, genes related to cytochrome P450 enzyme (and its isoforms), such as the aforementioned CYP1A2 gene, are currently widely used in hepatotoxicity studies due to their role in drug metabolism<sup>14, 16-18</sup>. For sake of a more comprehensive hepatotoxicity assessment, we describe in this paper our investigation into the feasibility of mRNA genes derived from Liver Function Tests’ protein biomarkers in hepatotoxicity assessment. In particular, two critical liver protein biomarkers<sup>19-22</sup> that we adopt herein are alanine transaminase<sup>20</sup> (ALT) and aspartate transaminase<sup>19</sup> (AST), where their elevations are often strongly suggestive of hepatocellular injury or liver damage. For example, an abnormal increase in the AST/ALT ratio of  $\geq 4$ -5x during drug therapy is often indicative of hepatotoxicity<sup>23</sup>. Additionally, by using said GOIs, our microfluidic NAT device may be applied to other applications, for example liver disease classification<sup>1</sup>, wherein different liver diseases often have different AST/ALT ratios. To the best of our knowledge, the approach embodying the application of microfluidic NAT based on the protein biomarkers used in Liver Function Tests is presently unreported and largely unexplored.

Collectively, we describe in this paper our proposed microfluidic NAT system, designed for a practical POCT hepatotoxicity assessment, embodying three functions: tissue sample preparation, multiplex RT-PCR and real-time fluorescent detection for gene expression analysis. To establish its feasibility for an *ex-vivo* hepatotoxicity assessment, laboratory mice are subjected to a short-term drug toxicity study, wherein cyclophosphamide, an alkylating agent often used in the cancer therapy and treatment of autoimmune disorders<sup>24</sup>, is administered in varying dosages. In our experiments, we are able to obtain high purity mRNA extracts, and illustrate that the final cDNA concentrations of AST and ALT increased by 58.7% and 33.3% respectively after 3x drug dosage

treatment. This demonstrates the validity of our selected mRNA gene targets in hepatotoxicity assessment. Moreover, our integrated microfluidic NAT system illustrates normalized fold changes of 1.62 and 1.31 for AST and ALT respectively during gene expression analysis. The results from our LOC system and from conventional methodology are largely consistent, thereby demonstrating the viability of using microfluidic NAT in POCT hepatotoxicity assessment.

## 1. Materials and methods

In this section, we will first delineate the protocols involved in our preclinical drug toxicity study to investigate the effects of hepatotoxicity. Secondly, we will discuss the design and assembly of our semi-integrated microfluidic chips for sample preparation and mRNA extraction, and for multiplex RT-PCR. Thirdly, we will delineate the primer preloading procedure carried out to prepare the RT-PCR microfluidic chip, followed by describing the microfluidic sample preparation and multiplex RT-PCR protocols. Lastly, we will discuss the fluorescence detection of amplified cDNA, including the duplex amplification of the two GOIs and their ensuing gene expression analysis.

### 2.1 Biological samples

A short-term (5 days) preclinical drug toxicity study was performed on common black laboratory mice (Strain name: C57BL/6J; Age: 5-7 weeks). All experiments were performed in accordance with the National Institutes of Health Guide for the care and use of laboratory animals (NIH Publications No. 80-23, revised 1996) and conducted after approval by the Institutional Animal Care and Use Committee of Houston Methodist Research Institute (HMRI).

A total of eight mice were divided into two equal groups, with one mouse in each group designated as the control and the remaining three subjected to drug treatment. The drug used was cyclophosphamide (200mg/kg body wt.)<sup>25</sup>, and the control used was saline with concentration of 0.9% w/v NaCl. The drug was administered through intraperitoneal route, with the first group having a single dose administered on the 1<sup>st</sup> day only; and the second group having 3 doses administered on the 1<sup>st</sup>, 3<sup>rd</sup> and 5<sup>th</sup> days. The animals were subsequently euthanized following standard carbon dioxide anaesthesia procedure on the 5<sup>th</sup> day after final drug administration. The mouse liver tissues were thereafter silated, and cut into equal small pieces (~20-30mg) and stored in RNAlater RNA Stabilization Reagent (Qiagen<sup>®</sup>, USA) at 4°C to prevent RNA degradation.

### 2.2 Sample preparation and mRNA extraction chip design and fabrication

Our proposed poly(methyl methacrylate) (PMMA) microfluidic chip for the sample preparation and mRNA extraction is depicted in Fig. 1a. The microfluidic chip (and subsequent RT-PCR microfluidic chip) was designed using Solidworks<sup>™</sup> software and comprised five PMMA layers (Fig. 1b) patterned using CO<sub>2</sub> laser ablation with a 35W CO<sub>2</sub> laser (VersaLASER VLS2.30, Universal<sup>®</sup> Laser Systems, USA). Each PMMA layer was subsequently cleaned in a bath sonicator with 10% v/v isopropanol for 15 minutes and dried in a vacuum oven at 80°C overnight. All five layers were clamped between two pieces of 5mm thick borosilicate glass pieces and thermally bonded in an oven at 128°C under a 1atm pressure for 2hrs, followed by natural cooling to room temperature.

The proposed PMMA chip comprised four main components (see Fig. 1a) which were all largely patterned in the 3<sup>rd</sup> PMMA layer, including a tissue lysis chamber, five reagent reservoirs, a mixing chamber, and seven mechanical valves. The tissue lysis chamber had a volume of ~250 $\mu$ L, and worked in conjunction with a tissue microhomogenizer attachment (ClaremontBio<sup>®</sup>, USA) which shredded and homogenized liver tissue samples placed within the chamber. Furthermore, an array of micro-pillars with dimensions 500 $\mu$ m x 500 $\mu$ m helped to remove any unwanted tissue debris from homogenized tissue lysate.

Our chip design included four reagent reservoirs with volumes of 450 $\mu$ L to preload and store buffers, and another 150 $\mu$ L reagent reservoir for the paramagnetic microbeads from the Dynabeads<sup>®</sup> mRNA DIRECT<sup>™</sup> Purification Kit (Ambion<sup>®</sup>, USA). During the mRNA extraction process, these buffers and microbeads were actuated from their respective reservoirs using external syringes.

For fluidic manipulation and control, mechanical valves were incorporated into our microfluidic chip. The mechanical force exerted by the external screws (see Fig. 1b) allowed the flexible 0.25mm thick silicon membrane (BISCO<sup>®</sup> Silicones, Rogers Corporation, USA, catalogue number HT-6240) to be directly deformed, thereby blocking microchannels and preventing solutions from passing through<sup>26</sup>.

Lastly, the mixing chamber had a volume of 150 $\mu$ L, and had the critical function of mixing the tissue lysate with the microbeads and relevant buffers for mRNA purification and extraction. This mixing function was accomplished via an adopted aeroelasticity-based fluid agitation technique<sup>27, 28</sup> which used the spontaneous vibration of a silicone membrane (or diaphragm) induced by an external air flow.

### 2.3 Multiplex RT-PCR chip design and fabrication

The proposed PMMA chip consisted of 12 reaction chambers connected to a central microchannel for multiplex RT-PCR reactions. Structurally, the RT-PCR reaction chambers were cut into the 1mm thick middle layer, and their top and bottom surfaces were enclosed respectively by 0.5mm thick PMMA top and bottom layers. This construction ensured minimization of the surface roughness within the reaction chambers which would otherwise result in unwanted bubble formation during the PCR thermal cycling process<sup>29</sup>.

Our chip design comprised a single assay loading inlet with attached NanoPort<sup>™</sup> PEEK ferrule connectors (Upchurch Scientific<sup>®</sup>, USA) and 1/32" OD tubing. The RT-PCR assay derived from the upstream sample preparation microfluidic chip was actuated through this inlet, and was equally distributed into the 12 reaction chambers. Each reaction chamber had a volume of ~10 $\mu$ L, with microchannels of 5mm by 0.2mm to allow the RT-PCR assay to be loaded. To minimize the undesirable effect of evaporation and the formation of bubbles, transparent adhesive PCR film seal (ThermoScientific<sup>®</sup>, Singapore) was used to seal the vent outlets during the RT-PCR process.

### 2.4 Liver tissue sample preparation and mRNA extraction on microfluidic chip

For this procedure, all instruments, microfluidic chips and equipment used were first sterilized with the UltraClean<sup>®</sup> Lab Cleaner (Mo-Bio Laboratories<sup>®</sup>, USA) and the experiment performed in a biosafety level 2 cabinet to minimize the presence of RNases. To prepare the microfluidic chip for sample preparation, 150 $\mu$ L of Dynabeads<sup>®</sup> microbeads solution stored in the reagent reservoir was actuated into the mixing chamber using a

250 $\mu$ L Hamilton<sup>®</sup> glass syringe (Sigma-Aldrich<sup>®</sup>, Singapore, catalogue number 24538-U), and a programmable syringe pump (New Era Pump Systems<sup>®</sup> Inc., USA, model number NE-1002x) at a flow rate of 100 $\mu$ L/min (see Fig. 3, Dynabeads<sup>®</sup> microbeads). 450 $\mu$ L Lysis/Binding buffer stored in another reagent reservoir on the chip was actuated into the mixing chamber to pre-condition the microbeads for subsequent mRNA binding. The mixing function was provided by the aeroelastic vibrational action of a thin-film silica diaphragm caused by the external air compressor<sup>27,28</sup>. Once the paramagnetic microbeads were pre-conditioned, the excess Lysis/Binding buffer was actuated into the Waste Collection Eppendorf tube whilst the microbeads were held within the mixing chamber with external neodymium magnets.

A liver tissue sample, weighing approximately 20-30mg, was loaded directly into the tissue lysis chamber. The tissue sample was secured within the chamber when the tissue microhomogenizer attachment was fitted into the opening of the lysis chamber. Subsequently, 250 $\mu$ L Lysis/Binding buffer was loaded into another 250 $\mu$ L glass syringe (see Fig. 3, Sample Inlet), and actuated into the tissue lysis chamber at a flow rate of 200 $\mu$ L/min. For tissue lysis, the microhomogenizer attachment was activated for ~1min to allow the liver tissue to be shredded and homogenized. After the completion of tissue lysis, the unwanted tissue debris and supernatant were removed by the micro-pillars as the homogenized tissue lysate was actuated into the mixing chamber, where the lysate was mixed with the microbeads for ~8mins to allow for mRNA binding.

The subsequent mRNA extraction and purification steps were performed using 450 $\mu$ L Washing buffers A/B as per a modified version of the manufacturer's suggested protocol, with a final extraction volume of 30 $\mu$ L (using the Elution buffer). The purified mRNA from each mouse liver tissue sample was collected in an Eppendorf tube preloaded with an RT-PCR master mix. To validate the efficacy of our sample preparation microfluidic chip, purified mRNA solutions extracted using our microfluidic chip was tested for their purity using the Nanodrop<sup>™</sup> 2000 (ThermoScientific<sup>®</sup>, Singapore), to ensure an A260/280 ratio of ~2.0-2.2 before proceeding to the subsequent downstream applications of RT-PCR and nucleic acid detection.

### 2.5 Preloading of PCR primers on microfluidic chip

Both forward and reverse primers of our two GOIs (AST and ALT) and our housekeeping gene  $\beta$ -actin were preloaded through the vent outlets/primer loading inlets (Fig. 1a) after the PMMA microfluidic chip had been thermally bonded and sterilized under ultraviolet (UV) radiation for 15 minutes. 50 $\mu$ M of each primer (forward and reverse) was diluted in nuclease-free water to make up a final-volume of 10 $\mu$ L and final-primer concentration of 0.5 $\mu$ M. The preloading process was performed using a micropipette, and the 12 chambers were separated into three groups to be treated with the AST, ALT and  $\beta$ -actin primer pairs respectively. Subsequently, the preloaded chip was dried in a convection oven at 65°C for 15 minutes to allow the water in the primer solution to evaporate, leaving the dried primers deposited as powder form in the individual reaction chambers. This surface treatment process would allow simultaneous amplification of multiple GOIs with a single RT-PCR assay.

### 2.6 Multiplex RT-PCR on microfluidic chip

Once the purified mRNA had been extracted from the liver tissue samples, 30 $\mu$ L of the purified mRNA extract (i.e. elution buffer with the microbeads) was collected in an Eppendorf tube containing the following RT-PCR

composition: 75 $\mu$ L 2x SYBR Green RT-PCR reaction mix (BioRad<sup>®</sup>, Singapore), 3.0 $\mu$ L iScript One-Step RT-PCR reverse transcriptase (BioRad<sup>®</sup>, Singapore) and 42 $\mu$ L nuclease-free water. This 150 $\mu$ L final RT-PCR assay was subsequently transferred from the Eppendorf tube into a 250 $\mu$ L Hamilton<sup>®</sup> glass syringe connected to the RT-PCR microfluidic chip via a 1/32" OD tubing.

To demonstrate the functionality of our multiplex RT-PCR microfluidic chip, the purified mRNA extracted from the mouse liver tissue samples were subjected to thermal cycling on our chip-compatible aluminium block thermal cycler. Our chip-compatible thermal cycler was based on the open-source OpenPCR<sup>®</sup> (Chai Biotechnologies, USA) platform, using a custom-designed aluminium metal block for contact-based thermal cycling and an Arduino microcontroller for precise temperature control (see Fig. 4).

For multiplex gene expression analysis, two different GOIs (i.e. AST and ALT) were amplified concurrently in each experimental run. The subsequent final cDNA concentrations of said GOIs were compared between the animals with and without drug treatment for gene expression analysis. Intron spanning primers were used for our two GOIs to ensure specific amplification of the transcribed mRNA and not the genomic DNA (see Table 1). Our AST and ALT primers were designed using the PrimerQuest software (Integrated DNA Technologies<sup>®</sup>, Singapore) and synthesized *de novo* from the same company. For our housekeeping gene,  $\beta$ -actin was selected and used in our qPCR experiments for normalization of data.  $\beta$ -actin is a common housekeeping gene that is widely used as a positive control in qPCR of mouse tissues due to its constitutive expression<sup>30,31</sup>. The  $\beta$ -actin primer assay was obtained from Qiagen<sup>®</sup>, Singapore (Catalog No. PPM02945B), with a band size of 154bp.

To prepare the microfluidic chip for multiplex RT-PCR, the RT-PCR assay was actuated into the 12 reaction chambers using a programmable syringe pump at a flow rate of 50 $\mu$ L/min. Once all 12 reaction chambers were sequentially filled with the RT-PCR assay, their vent outlets were sealed with the aforementioned transparent adhesive PCR film seal. Subsequently, 30 $\mu$ L of an immiscible PCR-grade mineral oil (Sigma-Aldrich<sup>®</sup>, Singapore) was actuated using the syringe pump to remove the excess RT-PCR assay remaining in the central microchannel (into the waste reservoir). The separation of the RT-PCR assays in individual reaction chambers by the immiscible mineral oil prevents any cross-contamination during the thermal cycling process. The sequence of events illustrating the microfluidic chip preparation process is depicted in Fig. 5.

To provide a benchmark reference to our chip, the same RT-PCR assays (with addition of forward/reverse primers at 0.5 $\mu$ M concentration) were amplified separately in Eppendorf tubes on a conventional CFX96 Touch<sup>™</sup> Real-Time PCR Detection System (BioRad<sup>®</sup>, USA).

The thermal cycling process was as follows: 70°C for 2mins to allow dehybridization of the captured mRNA from the microbeads, followed by 50°C for 10 minutes for reverse transcription, subsequently with an initial denaturation step of 95°C for 5mins and finally 35 cycles of PCR, comprising two stages: denaturation at 95°C for 10s and annealing/extension at 55°C for 30s.

## 2.7 Fluorescent detection of amplified cDNA

To enable simultaneous fluorescent detection of amplified cDNA for a fully-quantitative methodology, we developed an image capturing system embodying a camera module with blue excitation LEDs to be mounted on

our chip-compatible thermal cycler (Fig. 6). A 3MP CMOS camera with mounted 550nm longpass optical filter (Island Optical Systems<sup>®</sup>, Singapore) was fitted onto a black opaque acrylic frame with a 470nm blue LED module (IORodeo<sup>®</sup>, USA) to provide an excitation source for the SYBR Green 1 fluorescent dye present in the RT-PCR assay. The blue LED module was affixed at an angle of  $\sim 45^\circ$  to the plane of the microfluidic chip to minimize excitation light interference on the captured light pathway of the camera unit.

Fluorescence images were captured during the annealing/extension phase (55°C) of each RT-PCR cycle<sup>32-34</sup> and the mean intensity from each reaction chamber was measured subsequently after RT-PCR completion using ImageJ image processing and analysis software. A standardized rectangular region (of fixed area) was used to select the fluorescence emission intensities from each reaction chamber, followed by using the measurement analysis tool to obtain the mean fluorescence intensities from the selected region of each chamber. The fluorescence intensity results were then plotted into real-time PCR amplification curves to allow us to perform gene expression analysis on said GOIs.

To evaluate the specificity of our multiplex RT-PCR process, the amplified PCR products were also visualized and analysed off-chip using conventional gel electrophoresis with a 3.0% agarose gel (Tris-acetate-EDTA or TAE) prestained with ethidium bromide (BioRad<sup>®</sup>, Singapore). The gels were typically run for 45 minutes at a constant voltage of 100V in 1X TAE buffer.

## 2. Results and discussions

In this section, we discuss the results obtained from the experiments delineated in the previous section. Firstly, we will discuss the feasibility of microfluidic sample preparation and mRNA extraction in terms of the purity of the mRNA solution. Secondly, we will discuss the viability of dried preloaded primers in PMMA chips in RT-PCR after re-suspension in reagent assay, as well as determining the optimum final-primer concentration to be preloaded. Thirdly, we will analyze the PCR amplification specificity and efficiency of our on-chip RT-PCR system by performing off-chip gel electrophoresis on amplified PCR products extracted from the chip after RT-PCR completion. Finally, we will examine the feasibility and functionality of our image capturing system integrated with our microfluidic RT-PCR system for real-time fluorescent detection to establish a proof-of-principle for a POCT NAT-based hepatotoxicity assessment device.

### 3.1 Microfluidic sample preparation and mRNA extraction

The Dynabeads<sup>®</sup> microbeads used in our microfluidic mRNA extraction protocols were coated with oligo (dT)<sub>25</sub> residues to allow for base binding with the polyA tails at the 3' end of most mRNA polynucleotides, hence resulting in an highly specific isolation protocol. Rather than the capture of total RNA<sup>14, 35</sup>, the specific capture of mRNA molecules would ensure a more relevant nucleic acid sample material for ensuing gene expression analysis.

To validate the feasibility of microfluidic sample preparation and mRNA extraction, we compared the purity of the mRNA extracts obtained from our microfluidic chips as well as from the conventional manual process of using the purification kit. The purity of an RNA sample can be quantified by measuring its absorbance in a spectrophotometer (e.g. Nanodrop<sup>™</sup> 2000) at different wavelengths of light (i.e. 260nm and 280nm)<sup>36</sup>.

Specifically, the ratio of absorbance of an RNA aliquot at 260nm and 280nm is used to assess its purity where an A260/280 ratio of  $\sim 2.14$  is largely considered to be a pure RNA sample dissolved in Tris-EDTA (TE) buffer at pH 8 (which is the base component of the elution buffer)<sup>36</sup>. Lower values are often indicative of the presence of contaminants, such as proteins and phenols, which are strongly absorbent near or at the 280nm wavelength.

Fig. 7 depicts the comparison of the purity of mRNA extracts between our microfluidic device and manual extraction method from 5 random mouse tissue samples. We observed that the best-fit horizontal mean from microfluidic mRNA extraction and from manual extraction mRNA extraction had an A260/280 ratio of  $\sim 2.17$  and  $\sim 2.05$  respectively. This indicated that the purity of our microfluidic mRNA extracts was considerably better than the manual mRNA extracts. This noticeable improvement in mRNA purity could be attributed to the sterile enclosed environment provided by on-chip preparation and extraction procedures. The increased quality of the purified mRNA would subsequently ensure more specific and more efficient cDNA amplification in the downstream RT-PCR process. In addition, our microfluidic mRNA extraction protocols also reduced the number of handling steps compared to the manual extraction process, and avoided unnecessary exposure to the external contaminants.

### 3.2 Re-suspension of dried preloaded primers

To perform on-chip RT-PCR, the RT-PCR assay (comprising purified mRNA hybridized to the microbeads and RT-PCR master mix) was loaded into our RT-PCR microfluidic chip and distributed to the 12 reaction chambers to mix with the different sets of dried primers during re-suspension. During the re-suspension process, the chip was left to stand at room temperature for 10 minutes to allow the dried primers to passively fully dissolve in the reagent assay. Active mixing was not performed to avoid any bubble generation which would otherwise result in uneven heat distribution within the reaction assay during thermal cycling.

During our experiments, there were concerns regarding the viability of the primers maintaining their nucleotide structure and functional integrity when exposed to high temperatures during the drying process. If the primer concentrations decreased due to high heat degradation, the efficiency of PCR would drop significantly<sup>37</sup>. To verify that the primers maintain their intended functionalities after being subjected to high temperatures, different concentrations of preloaded primers were tested using the ALT target gene and corresponding primers.

Fig. 8 depicts the differences in PCR amplification efficiencies after on-chip thermal cycling of varying final concentrations of the re-suspended dried primers. From Fig. 8, we observed that high temperature treatment on the primers during the drying process did not have any adverse effect on the functional integrity of the primers. In Fig. 8b, we also observed that the signal intensity of the amplified DNA product after gel electrophoresis saturated at a final-primer concentration of  $0.5\mu\text{M}$  and higher, indicating that we were able to preload an optimum final-primer concentration of  $0.5\mu\text{M}$  in the chip without any loss in primers functionality after the drying process.

The process of preloading the primers in dried form was critical towards the design of a microfluidic chip. In our microfluidic chip design, we were able to incorporate a single assay loading inlet to distribute the RT-PCR assays into different reaction chambers preloaded with different primer sets. This surface treatment procedure

removed the need to pre-mix different primer sets for multiple RT-PCR assays, thereby significantly simplifying off-chip handling procedures (particularly for multiplex gene expression analysis).

### 3.3 Microfluidic multiplex RT-PCR

Multiple RT-PCR was verified on our PMMA microfluidic chip embodying 12 reaction chambers, preloaded with 0.5 $\mu$ M final-primer concentrations. Each microfluidic multiplex RT-PCR run embodied a purified mRNA extract from a single liver tissue sample targeting our two GOIs (i.e. AST and ALT) and our housekeeping gene (i.e.  $\beta$ -actin).

To ascertain the specificity of our multiplex RT-PCR reactions, the RT-PCR amplicons were extracted from the chip and analyzed off-chip using conventional gel electrophoresis (see Fig. 9). We observed three clear bands on the agarose gel electrophoresis image for each replicate group (for a total of 12) in Fig. 9, wherein the bands at 221-bp, 182-bp and 154-bp belonged to the ALT, AST and  $\beta$ -actin target fragments respectively. This clear band separation with minimal band smearing indicated that our multiplex RT-PCR reaction was highly specific, and verified the usage of mineral oil as a separation medium to eliminate cross-contamination between reaction chambers.

In addition, the average signal intensities obtained from the gel electrophoresis image could be converted into an electropherogram and used for qualitative analysis of end-point RT-PCR<sup>14, 17</sup>. From the electropherograms, we were able to determine the differences in final cDNA concentrations from liver tissue samples with/without drug treatment, wherein the strength of signal intensities are proportional to the quantity of amplified gene product present<sup>37</sup>. This qualitative analytic technique could be used to estimate gene expression levels of our GOIs, and investigate any changes due to cyclophosphamide administration<sup>14</sup>. In Fig. 10, the signal intensities for the RT-PCR amplicons from the treated tissue samples (both 1x dosage and 3x dosage) were normalized to those from untreated control tissue sample. This allowed us to compare and average the data obtained from three biological replicates (i.e. each run encompassing one out of the three drug-treated mice from each treatment group). In view of the statistical significance for the drug-treated groups vis-à-vis the untreated controls, we performed a 2 way ANOVA statistical analysis. Our statistical analysis comprised the data obtained from three biological replicates and three technical replicates (from each treatment group), and depicted that the variations of our two GOIs were statistically difference (i.e. p-value <0.0001) between the drug-treated groups and untreated controls.

From Fig. 10, we observed that the differences in final cDNA concentrations at 1x drug dosage largely had no significant difference when compared to the untreated control samples. We speculated that this lack of increase in gene expressions levels at 1x drug dosage could be attributed to low (or delayed) drug metabolism of the administered drug in the mice<sup>38</sup>.

There were, however, significant increases in final cDNA concentrations for both AST and ALT at 3x drug dosage of cyclophosphamide (200mg/kg body wt.), with 58.7% and 33.3% increases for AST and ALT respectively. These results support our hypothesis of using a biomolecular diagnostic approach (or NAT) as a viable alternative to conventional Liver Function Tests. These elevations in gene expression levels were generally consistent with data from genetic testing using laboratory mice, wherein significant elevations (in particular ALT) were observed after excessive alcohol consumption<sup>21</sup> or in mouse fatty liver tissues<sup>22</sup>, and could

be used as evidence of hepatocellular damage. Additionally, we observed that  $\beta$ -actin mRNA expression levels remained relatively unchanged after a 1x and 3x drug dosage. These results illustrated the constitutive expression behavior of  $\beta$ -actin and helped to validate it as an appropriate choice of housekeeping gene and positive control for our qPCR experiments.

In a separate microfluidic experiment where DNA amplification was performed without the reverse transcription step, genomic contamination was observed to be kept to a minimum. Gel electrophoresis results showed no signal bands for both GOIs as well as the housekeeping gene, indicating the absence of an amplified PCR product. From this result, we were able to unambiguously demonstrate the validity of our intron-spanning primers used for AST, ALT and  $\beta$ -actin mRNA targets.

In short, the increase in genes expression levels for our two GOIs at 3x drug dosage validated the potential for using mRNA target genes based on Liver Function Tests protein biomarkers, and demonstrated the viability of a POCT NAT device for hepatotoxicity assessment.

### 3.4 Fluorescent detection and gene expression analysis

To evaluate the viability of our image capturing system in determining the differences in fluorescence emissions between RT-PCR assays targeting different GOIs, we performed real-time fluorescence emission image captures embodying the 12 reaction chambers. Fluorescence images were captured at each PCR cycle during the annealing/extension phase (55°C)<sup>32,33</sup> for a total of 35 cycles.

The intensities in fluorescence emissions derived from captured images were plotted in Fig. 11 to obtain a real-time fluorescence emission curve for both GOIs (i.e. AST and ALT) and the housekeeping gene (i.e.  $\beta$ -actin). With three biological replicates in each treatment group, we were able to account for variation between samples for more precise gene expression measurements<sup>39</sup>. From the real-time fluorescence amplification plots in Fig. 11, we were able to estimate the initial mRNA concentrations of our samples used via their respective average  $C_t$  values;  $C_t$  (or cycle threshold) values are often used in quantitative PCR as an indicator of starting/initial concentration of the nucleic acid template<sup>32,40,41</sup>.

To determine the number of cycles required for the fluorescence signal to exceed that of the background level<sup>42</sup>, the user-defined  $C_t$  threshold value in Fig. 11 was selected based on No Template Control (NTC) fluorescence intensities. Our  $C_t$  threshold was defined by post-experimental results analysis wherein the number of cycles required for the fluorescence intensities to cross a pre-determined fluorescence threshold (i.e. 20% higher than those of the NTCs) were consistent with the results obtained from a conventional real-time thermal cycler. The  $C_t$  values of all six samples (AST-control, AST-3x dosage, ALT-control, ALT-3x dosage,  $\beta$ -actin-control, and  $\beta$ -actin-3x dosage) were correspondingly interpolated and tabulated in Table 2, and compared to determine the relative changes in the mRNA initial concentrations. Table 2 shows that the average  $C_t$  value of AST on our microfluidic chip decreased from 20.5 to 19.9 after a 3x drug dosage, while the average  $C_t$  value of ALT decreased from 28.8 to 28.5. Conversely, the average  $C_t$  value of  $\beta$ -actin remained relatively constant – once again illustrating the constitutive expression behavior of our housekeeping gene.

The presence of the housekeeping gene,  $\beta$ -actin, allowed us to normalize our qPCR experimental data, to minimize possible variations from the experimental setup such as sample preparation and handling, reverse transcription efficiency between sample-sample/run-run repetitions, and DNA amplification efficiencies<sup>42, 43</sup>. To obtain a normalized target gene expression level, we used the Livak method<sup>42</sup> to first determine the difference in  $C_t$  values between a target gene and the housekeeping gene for a particular sample, before obtaining the  $\Delta\Delta C_t$  values (indicative of normalized fold change)<sup>42</sup>. From our microfluidic experimental data, we demonstrated that the normalized fold changes (or up-regulation) for AST and ALT were 1.62 and 1.31 respectively. These values largely indicated that the 3x drug dosaged samples had a higher concentration of initial nucleic acid (or target mRNA in our case) concentration when compared to an untreated control. In the perspective of the differences of up-regulations between AST and ALT, we observed that ALT had a relatively lower increase in gene expression levels compared to AST. We speculate that this might be due to the reduced (or delayed) response of ALT to cyclophosphamide administration (*vis-à-vis* AST). Nonetheless, our statistical analysis indicated that AST and ALT collectively illustrated significant differences between the 3x drug dosaged samples and untreated controls.

These results were consistent with the estimates of gene expression changes (i.e. 58.7% and 33.3% increases for AST and ALT respectively) from our previous qualitative analytic approach (derived from final cDNA concentrations). This consistency of up-regulated gene expression changes from both our qualitative analytic approach and fully-quantitative fluorescent detection methodology herein demonstrated the efficacy of the latter, and its integration with our microfluidic RT-PCR system. More importantly, we validated the AST and ALT GOIs derived from protein biomarkers used in Liver Function Tests, which were illustrated to have been up-regulated after 3x cyclophosphamide treatment.

Collectively, we have designed and demonstrated an integrated LOC system embodying tissue sample preparation, multiplex RT-PCR and real-time fluorescent detection for POCT hepatotoxicity assessment – hence the viability of POCT for hepatotoxicity assessment.

### 3. Conclusions

We have designed and implemented an LOC system that is somewhat close to a practical POCT hepatotoxicity assessment device, featuring semi-automation, relatively easy-to-use, and “sample-in-answer-out” capabilities for multiplex gene expression analysis. Our LOC system embodied the integration of tissue sample preparation, multiplex RT-PCR, and real-time fluorescent detection methodology, and its efficacy was validated by multiplex gene expression analysis on two GOIs (i.e. AST and ALT) derived from Liver Function Tests’ biomarkers.

The results from our microfluidic tissue sample preparation module integrated with our multiplex RT-PCR chip has yielded improved purity of mRNA extracts over manual extraction means while significantly reducing off-chip handling procedures for multiple gene targets. The GOIs derived from Liver Function Tests’ protein biomarkers validated by our microfluidic RT-PCR results have illustrated up-regulations in their gene expression levels (i.e. increased in final cDNA concentration by 58.7% and 33.3% for AST and ALT respectively) in mice liver tissue samples with a 3x dosage cyclophosphamide drug treatment. Further, our fully-

quantitative real-time fluorescent detection methodology has also demonstrated normalized fold changes of 1.62 and 1.31 for AST and ALT respectively, and these results were consistent with the results obtained from using bulky, conventional methodology.

In the terms of the equipment footprint of our integrated LOC system, it is not unexpected that size of our entire microfluidic setup is somewhat incompatible with the small footprint and portability criteria of POCT. Hence, in the perspective of future work on our integrated LOC system, we recommend further miniaturization of our entire setup and reduce the dependency on external instrumentations (in particular our tissue sample preparation module). Nonetheless, the aforementioned compatibility of our integrated LOC system with other criteria of POCT is an important step towards the realization of a practical POCT liver assessment device.

## Acknowledgements

The authors would like to thank our colleagues, Ms. Sharon Tan and Mr. Fan Wei, from the Microfluidics Manufacturing Programme in Singapore Institute of Manufacturing Technology (SIMTech, Singapore) for their helpful advice and assistance. The work involved in the preclinical toxicity study was also supported by Ms. Lilian Low and Ms. Zhou Tieling from The Methodist Hospital Research Institute (TMHRI, USA).

## References

1. K. R. Reddy and T. Faust, *The Clinician's Guide to Liver Disease*, SLACK Incorporated, 2006.
2. J. Blaha and S. Duarte, Histology Technology and Lean Healthcare Hand in Hand, <http://www.isixsigma.com/methodology/kaizen/histology-technology-and-lean-healthcare-hand-hand/>, Accessed 21 September 2014.
3. J. Ho, O. Aridor and A. V. Parwani, *Journal of pathology informatics*, 2012, **3**.
4. P. J. Santrach, *Current & Future Applications of Point of Care Testing*, Mayo Clinic, [www.cdc.gov](http://www.cdc.gov).
5. C. Zhang, J. Xu, W. Ma and W. Zheng, *Biotechnology Advances*, 2006, **24**, 243-284.
6. P. M. van Midwoud, E. Verpoorte and G. M. Groothuis, *Integrative biology : quantitative biosciences from nano to macro*, 2011, **3**, 509-521.
7. S. M. Hattersley, C. E. Dyer, J. Greenman and S. J. Haswell, *Lab Chip*, 2008, **8**, 1842-1846.
8. R. Baudoin, A. Corlu, L. Griscom, C. Legallais and E. Leclerc, *Toxicology in vitro : an international journal published in association with BIBRA*, 2007, **21**, 535-544.
9. K. Anderson, J. M. Cooper, S. J. Haswell, D. Marshall, H. Yin and X. Zhang, *The Analyst*, 2010, **135**, 1282-1287.
10. K. A. Hagan, C. R. Reedy, M. L. Uchimoto, D. Basu, D. A. Engel and J. P. Landers, *Lab on a Chip - Miniaturisation for Chemistry and Biology*, 2011, **11**, 957-961.
11. S. Pernagallo, G. Ventimiglia, C. Cavalluzzo, E. Alessi, H. Ilyine, M. Bradley and J. J. Diaz-Mochon, *Sensors (Switzerland)*, 2012, **12**, 8100-8111.
12. D. Chen, M. Mauk, X. Qiu, C. Liu, J. Kim, S. Ramprasad, S. Ongagna, W. R. Abrams, D. Malamud, P. L. A. M. Corstjens and H. H. Bau, *Biomedical Microdevices*, 2010, **12**, 705-719.
13. C. Zhang and D. Xing, *Nucleic Acids Research*, 2007, **35**, 4223-4237.
14. K. J. Shaw, E. M. Hughes, C. E. Dyer, J. Greenman and S. J. Haswell, *Lab Invest*, 2013, **93**, 961-966.

15. G. Jiang and D. J. Harrison, *The Analyst*, 2000, **125**, 2176-2179.
16. T. M. Bosch, A. D. R. Huitema, V. D. Doodeman, R. Jansen, E. Witteveen, W. M. Smit, R. L. Jansen, C. M. Van Herpen, M. Soesan, J. H. Beijnen and J. H. M. Schellens, *Clinical Cancer Research*, 2006, **12**, 5786-5793.
17. S. J. Baldwin, J. L. Bramhall, C. A. Ashby, L. Yue, P. R. Murdock, S. R. Hood, A. D. Ayrton and S. E. Clarke, *Drug metabolism and disposition: the biological fate of chemicals*, 2006, **34**, 1063-1069.
18. D. D. Vakharia, N. Liu, R. Pause, M. Fasco, E. Bessette, Q. Y. Zhang and L. S. Kaminsky, *Toxicology and applied pharmacology*, 2001, **170**, 93-103.
19. M. Lia, R. Barouki and S. G. Waelsch, *Proc Natl Acad Sci U S A*, 1995, **92**, 788-790.
20. W. J. Reagan, R. Z. Yang, S. Park, R. Goldstein, D. Brees and D. W. Gong, *Toxicologic pathology*, 2012, **40**, 1117-1127.
21. L. Sosa, D. Vidlak, J. M. Strachota, J. Pavlik and T. R. Jerrells, *International immunopharmacology*, 2005, **5**, 301-314.
22. S. B. Jadhao, R. Z. Yang, Q. Lin, H. Hu, F. A. Anania, A. R. Shuldiner and D. W. Gong, *Hepatology (Baltimore, Md.)*, 2004, **39**, 1297-1302.
23. R. J. Andrade, M. Robles, A. Fernandez-Castaner, S. Lopez-Ortega, M. C. Lopez-Vega and M. I. Lucena, *World journal of gastroenterology : WJG*, 2007, **13**, 329-340.
24. S. C. J. Yeung, C. P. Escalante and R. F. Gagel, *Medical Care of Cancer Patients*, People's Medical Publishing House, 2009.
25. E. Anton, *British journal of experimental pathology*, 1987, **68**, 237-249.
26. R. Mohan, B. R. Schudel, A. V. Desai, J. D. Yearsley, C. A. Apblett and P. J. A. Kenis, *Sensors and Actuators B: Chemical*, 2011, **160**, 1216-1223.
27. H. M. Xia, Z. P. Wang, W. Fan, A. Wijaya, W. Wang and Z. F. Wang, *Lab Chip*, 2012, **12**, 60-64.
28. H. M. Xia, Z. P. Wang, W. Wang, W. Fan, A. Wijaya and Z. F. Wang, *Lab on a Chip*, 2013, **13**, 1619-1625.
29. H. B. Liu, H. Q. Gong, N. Ramalingam, Y. Jiang, C. C. Dai and K. M. Hui, *Journal of Micromechanics and Microengineering*, 2007, **17**, 2055-2064.
30. K. E. Kouadjo, Y. Nishida, J. F. Cadrin-Girard, M. Yoshioka and J. St-Amand, *BMC Genomics*, 2007, **8**, 127.
31. E. d. L. Rebouças, J. J. d. N. Costa, M. J. Passos, J. R. d. S. Passos, R. v. d. Hurk and J. R. V. Silva, *Brazilian Archives of Biology and Technology*, 2013, **56**, 143-154.
32. Q. Xiang, B. Xu, R. Fu and D. Li, *Biomedical microdevices*, 2005, **7**, 273-279.
33. M. B. Sayers and T. M. Dalton, *A real-time continuous flow polymerase chain reactor for DNA expression quantification*, Seattle, WA, 2008.
34. N. Ramalingam, H. B. Liu, C. C. Dai, Y. Jiang, H. Wang, Q. Wang, K. M. Hui and H. Q. Gong, *Biomedical Microdevices*, 2009, **11**, 1007-1020.
35. L. VanHeirstraeten, P. Spang, C. Schwind, K. Drese, M. Ritzi-Lehnert, B. Nieto, M. Camps, B. Landgraf, F. Guasch and A. Corbera, *LAB ON A CHIP*, 2014, **14**, 1519-1526.
36. D. Liu, *Handbook of Nucleic Acid Purification*, CRC Press, 2009.
37. M. McPherson and S. Møller, *PCR*, Taylor & Francis, 2007.
38. S. C. Chow and J. Liu, *Design and Analysis of Animal Studies in Pharmaceutical Development*, Taylor & Francis, 1998.
39. E. Wit and J. McClure, *Statistics for Microarrays: Design, Analysis and Inference*, Wiley, 2004.
40. E. A. Oblath, W. H. Henley, J. P. Alarie and J. M. Ramsey, *Lab Chip*, 2013, **13**, 1325-1332.
41. N. Ramalingam, Z. Rui, H. B. Liu, C. C. Dai, R. Kaushik, B. Ratnharika and H. Q. Gong, *Sensors and Actuators, B: Chemical*, 2010, **145**, 543-552.
42. M. T. Dorak, *Real-time PCR*, Taylor & Francis, 2007.
43. Life Technologies Corporation, *Real-time PCR: Understanding Ct*.

## FIGURE LEGENDS

**Fig 1** Sample preparation microfluidic chip design: a) Schematic layout of the microfluidic chip indicating the various features; b) Model of the microfluidic chip in an exploded view illustrating the different PMMA layers, tissue microhomogenizer attachment for tissue lysis, mechanical screws/nuts and silicon membranes for valve control, and attached NanoPort™ ferrules for fluid input and actuation.

**Fig 2** RT-PCR microfluidic chip design: a) Schematic layout of the microfluidic chip indicating the various features; and b) Model of the microfluidic chip in an exploded view illustrating the different PMMA layers, aluminium heat block, and attached NanoPort™ ferrule.

**Fig 3** Schematic depicting the tissue sample preparation setup featuring a syringe pump, PMMA microfluidic chip with preloaded microbeads and buffers in reagent reservoir chambers, external Eppendorf tubes for collection, and an external air compressor to provide a chamber mixing function.

**Fig 4** Schematic depicting the multiplex microfluidic RT-qPCR setup featuring a syringe pump, PMMA microfluidic chip on an aluminium heater connected to an Arduino microcontroller, and 3MP CMOS camera module with 550nm longpass filter and 470nm blue excitation LEDs connected to a computer.

**Fig 5** Illustration of RT-PCR microfluidic chip preparation with colored dye and brown adhesive tape: a) Loading of RT-PCR assay into single loading inlet to be sequentially distributed into preloaded reaction chambers; b) Sealing of vent outlets and loading of immiscible mineral oil to separate individual reaction chambers to prevent cross-contamination.

**Fig 6** RT-PCR and fluorescent detection setup: Photograph of entire microfluidic setup with a chip-compatible thermal cycler and attached fluorescent detection module.

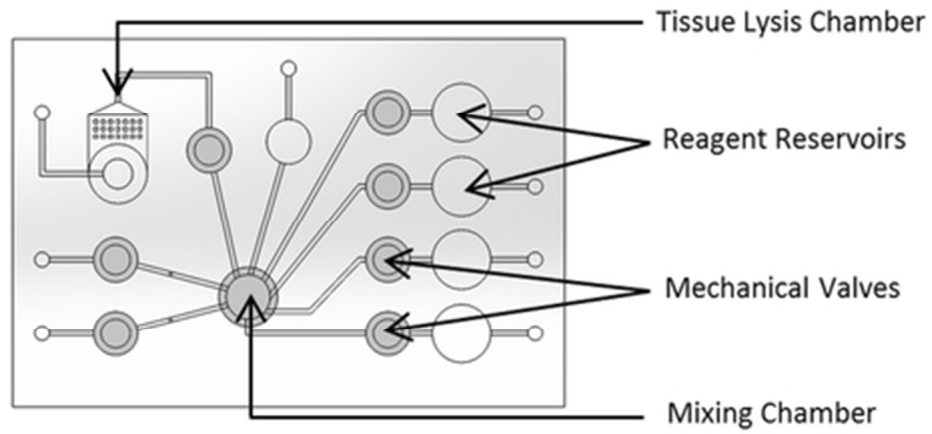
**Fig 7** Comparison of A260/280 ratios as a measure of mRNA purity between microfluidic and manual extraction methods from five random mouse tissue samples.

**Fig 8** Re-suspension of dried preloaded primers with varying final concentrations in RT-PCR reagent assay for ALT target gene followed by on-chip thermal cycling: a) Gel electrophoresis image showing varying final-primer concentrations (0.1μM, 0.25μM, 0.5μM, 0.75μM and 1.0μM) against a 100bp DNA ladder; b) Signal intensity plot (r.f.u) against final-primer concentration using data derived from gel electrophoresis electropherogram plots. Experiments were performed in triplicates, with error bars shown accordingly.

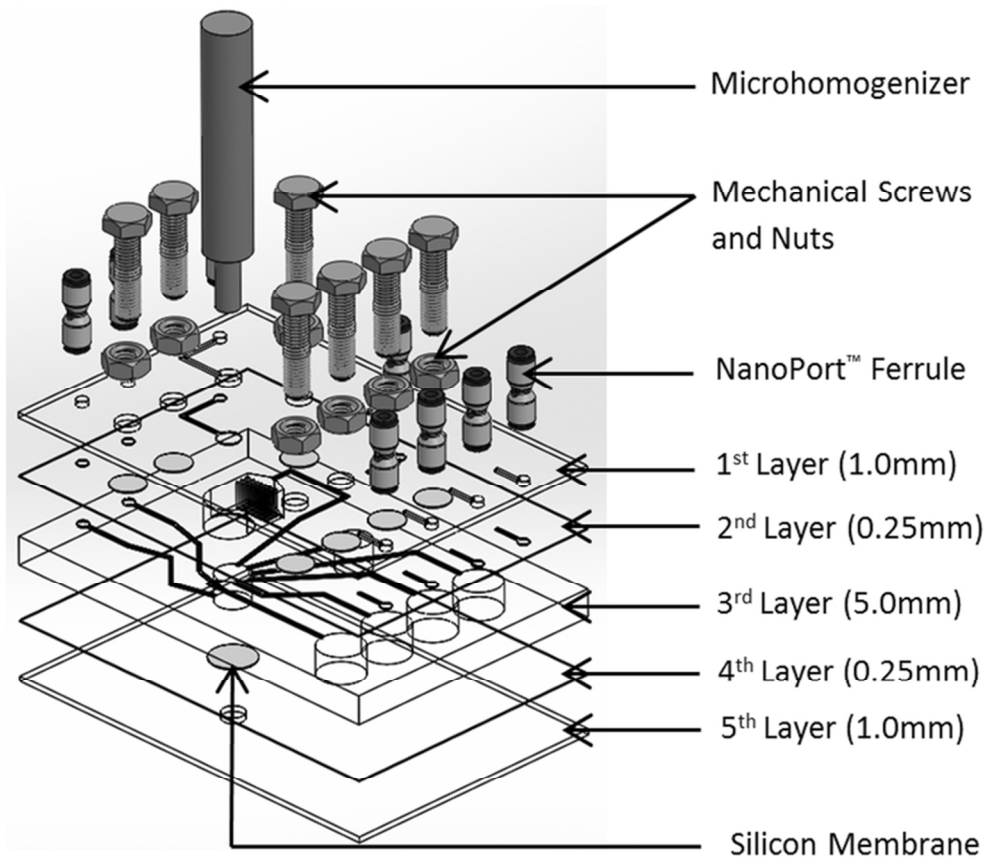
**Fig 9** Agarose gel electrophoresis image taken under trans-UV illustrating the specificity of multiplex RT-PCR targeting both ALT and AST genes of interests, and β-actin housekeeping gene from 3x-dosaged mice liver tissue samples. The 12 reaction chambers on our microfluidic chip allowed four replicate groups, each with three target fragments.

**Fig 10** Comparison of the differences in AST, ALT and β-actin cDNA concentrations after varying levels (1x and 3x) of drug treatment (cyclophosphamide, 200mg/kg body wt.). Experiments were performed in triplicates, with results normalized to the untreated control.

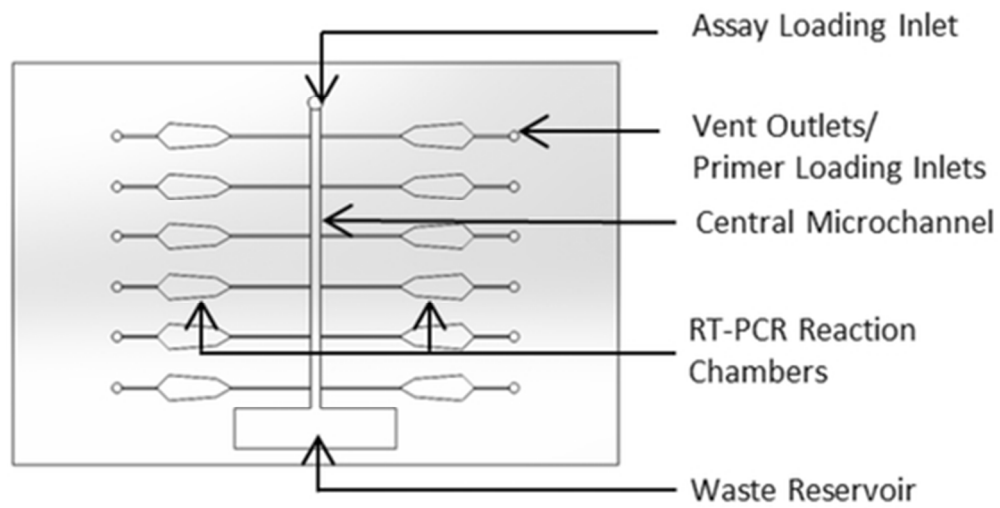
**Fig 11** Quantification of real-time fluorescence emission for a) AST, b) ALT and c) β-actin at 3x drug dosage using ImageJ, with images captured at the annealing/extension phase of each PCR cycle.



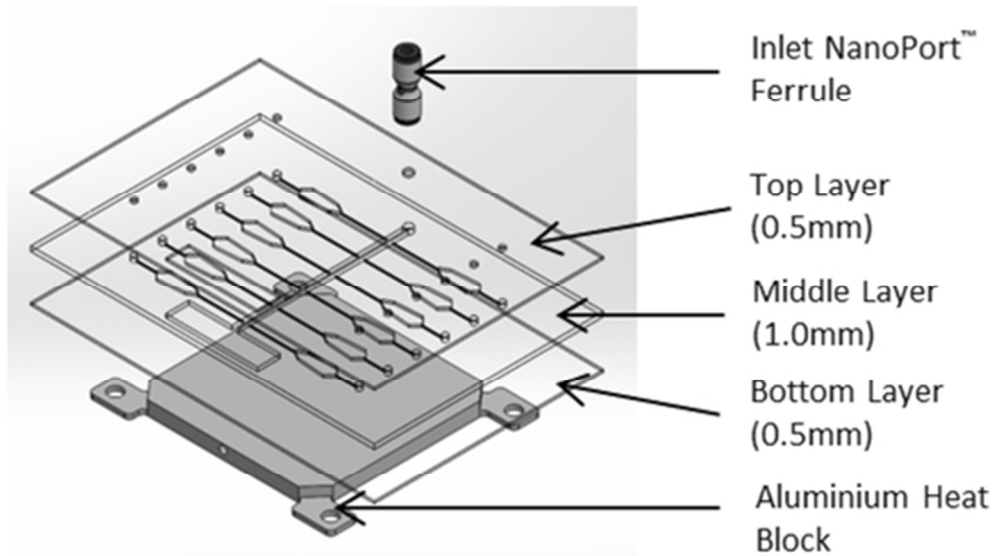
Sample preparation microfluidic chip design: a) Schematic layout of the microfluidic chip indicating the various features; b) Model of the microfluidic chip in an exploded view illustrating the different PMMA layers, tissue microhomogenizer attachment for tissue lysis, mechanical screws/nuts and silicon membranes for valve control, and attached NanoPort™ ferrules for fluid input and actuation.  
38x18mm (300 x 300 DPI)



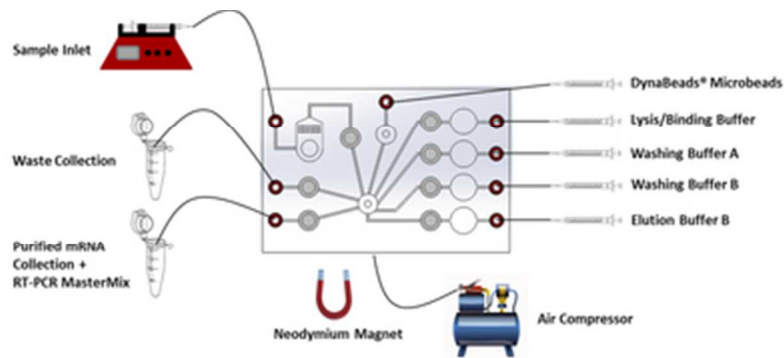
Sample preparation microfluidic chip design: a) Schematic layout of the microfluidic chip indicating the various features; b) Model of the microfluidic chip in an exploded view illustrating the different PMMA layers, tissue microhomogenizer attachment for tissue lysis, mechanical screws/nuts and silicon membranes for valve control, and attached NanoPort™ ferrules for fluid input and actuation.  
72x64mm (300 x 300 DPI)



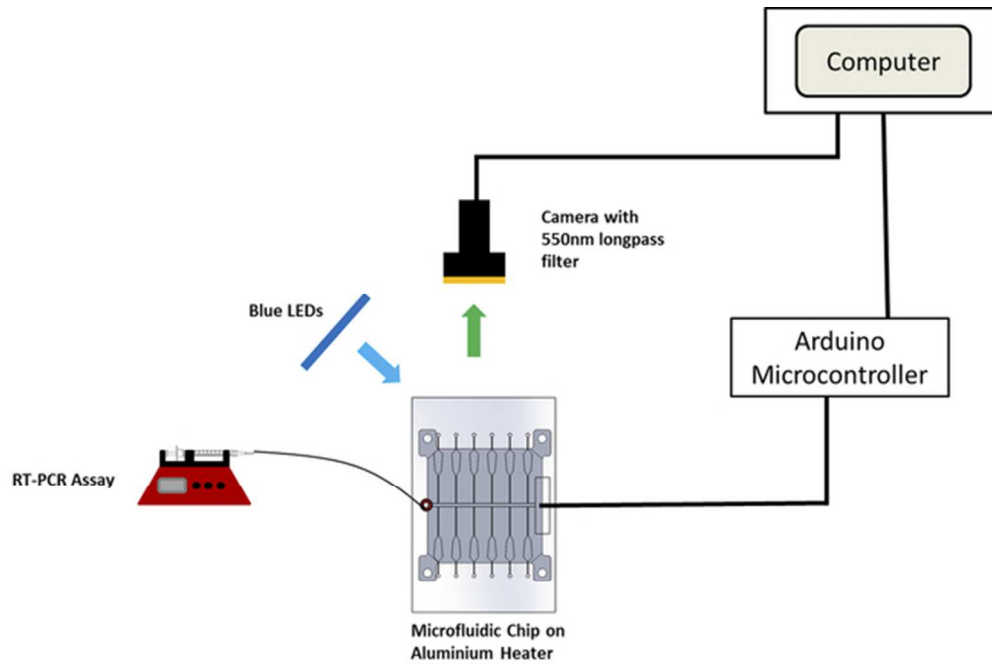
RT-PCR microfluidic chip design: a) Schematic layout of the microfluidic chip indicating the various features; and b) Model of the microfluidic chip in an exploded view illustrating the different PMMA layers, aluminium heat block, and attached NanoPort™ ferrule.  
42x22mm (300 x 300 DPI)



RT-PCR microfluidic chip design: a) Schematic layout of the microfluidic chip indicating the various features; and b) Model of the microfluidic chip in an exploded view illustrating the different PMMA layers, aluminium heat block, and attached NanoPort™ ferrule.  
46x26mm (300 x 300 DPI)



Schematic depicting the tissue sample preparation setup featuring a syringe pump, PMMA microfluidic chip with preloaded microbeads and buffers in reagent reservoir chambers, external Eppendorf tubes for collection, and an external air compressor to provide a chamber mixing function.  
35x14mm (300 x 300 DPI)



Schematic depicting the multiplex microfluidic RT-qPCR setup featuring a syringe pump, PMMA microfluidic chip on an aluminium heater connected to an Arduino microcontroller, and 3MP CMOS camera module with 550nm longpass filter and 470nm blue excitation LEDs connected to a computer.  
55x37mm (300 x 300 DPI)

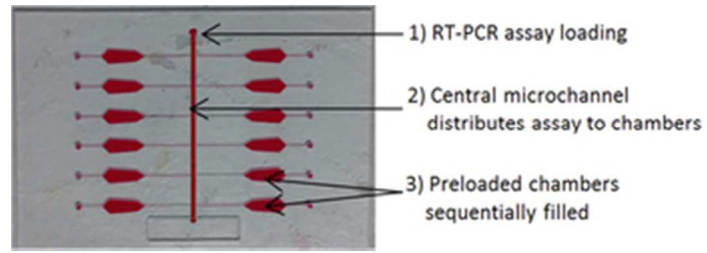


Illustration of RT-PCR microfluidic chip preparation with colored dye and brown adhesive tape: a) Loading of RT-PCR assay into single loading inlet to be sequentially distributed into preloaded reaction chambers; b) Sealing of vent outlets and loading of immiscible mineral oil to separate individual reaction chambers to prevent cross-contamination.  
29x10mm (300 x 300 DPI)

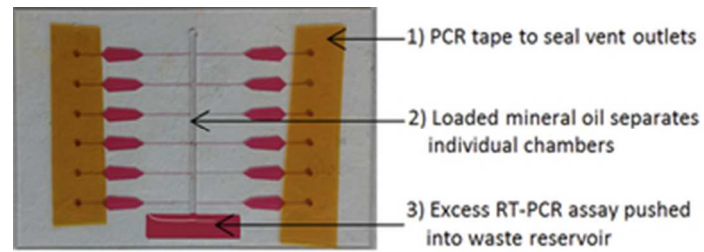
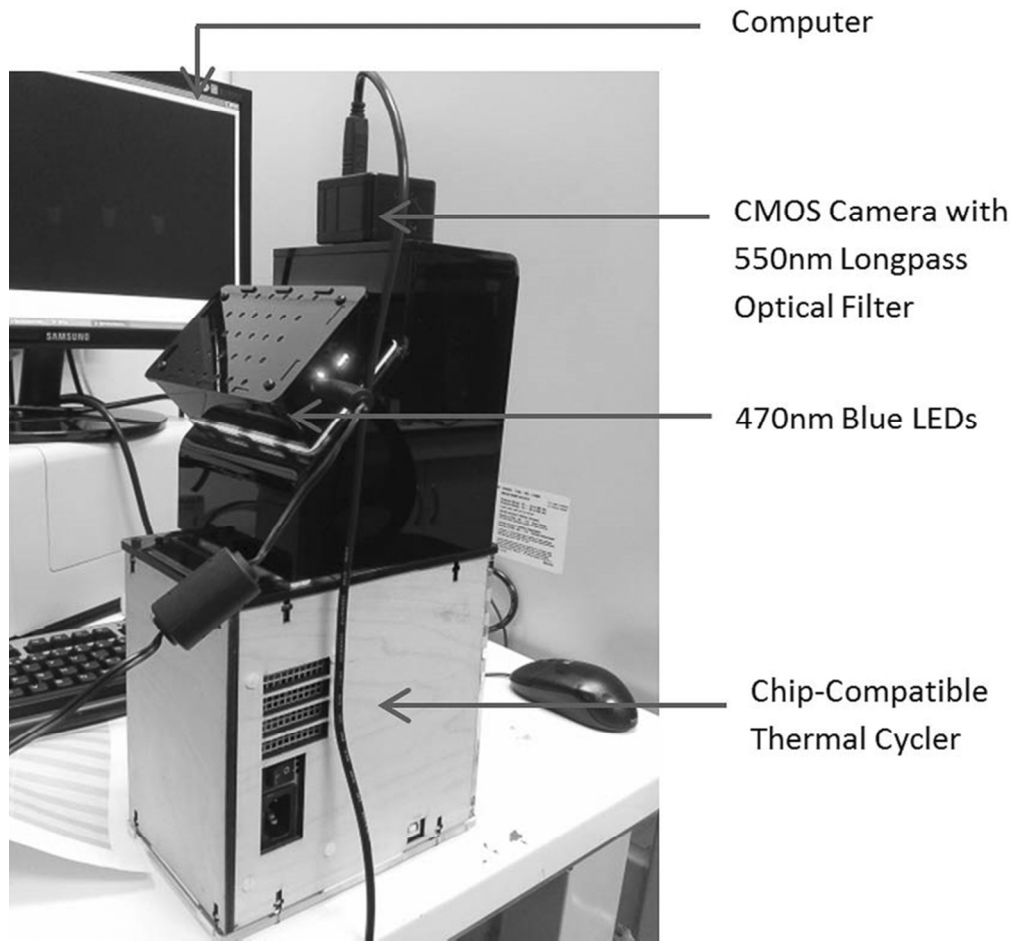
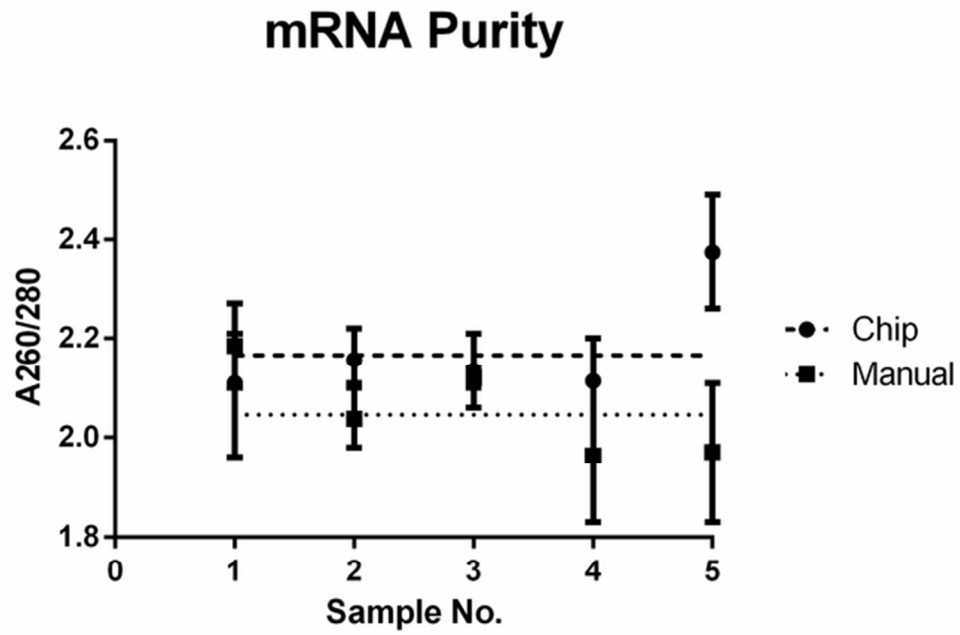


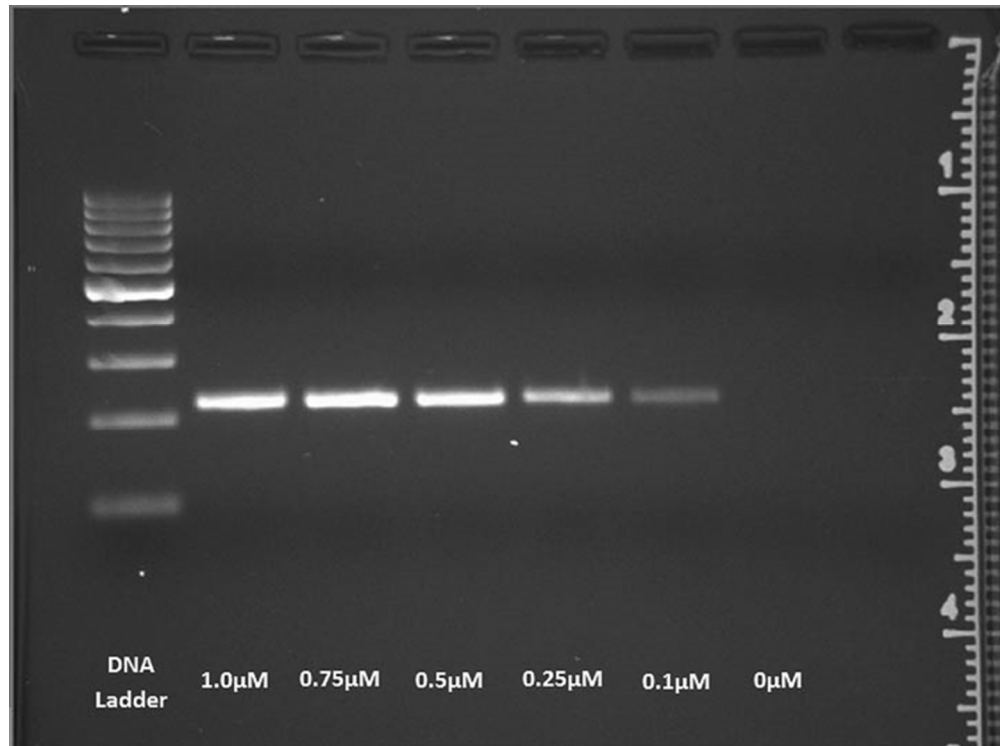
Illustration of RT-PCR microfluidic chip preparation with colored dye and brown adhesive tape: a) Loading of RT-PCR assay into single loading inlet to be sequentially distributed into preloaded reaction chambers; b) Sealing of vent outlets and loading of immiscible mineral oil to separate individual reaction chambers to prevent cross-contamination.  
29x10mm (300 x 300 DPI)



RT-PCR and fluorescent detection setup: Photograph of entire microfluidic setup with a chip-compatible thermal cycler and attached fluorescent detection module.  
77x72mm (300 x 300 DPI)

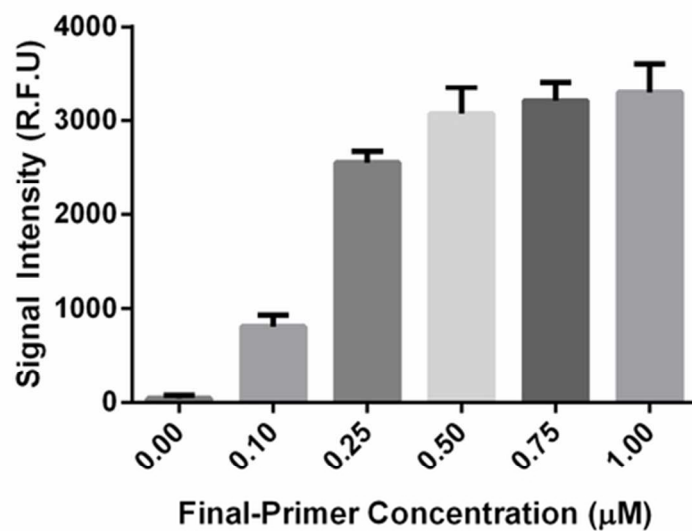


Comparison of A260/280 ratios as a measure of mRNA purity between microfluidic and manual extraction methods from five random mouse tissue samples.  
57x39mm (300 x 300 DPI)

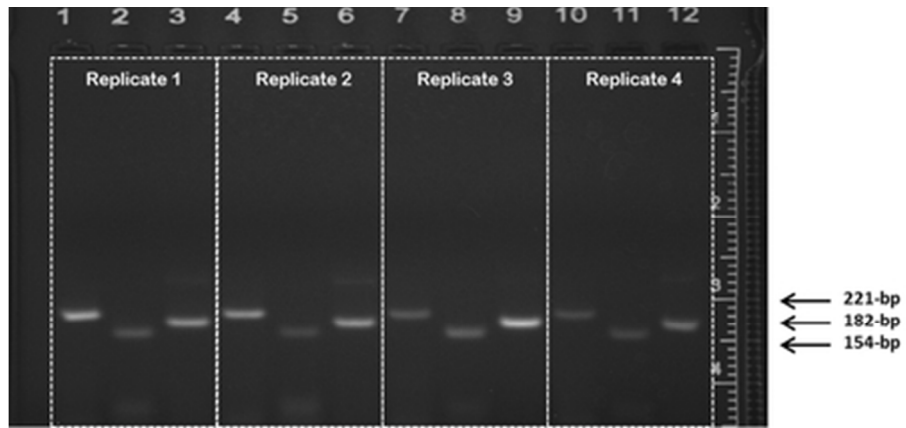


Re-suspension of dried preloaded primers with varying final concentrations in RT-PCR reagent assay for ALT target gene followed by on-chip thermal cycling: a) Gel electrophoresis image showing varying final-primer concentrations (0.1 μM, 0.25 μM, 0.5 μM, 0.75 μM and 1.0 μM) against a 100bp DNA ladder; b) Signal intensity plot (r.f.u) against final-primer concentration using data derived from gel electrophoresis electropherogram plots. Experiments were performed in triplicates, with error bars shown accordingly.  
61x45mm (300 x 300 DPI)

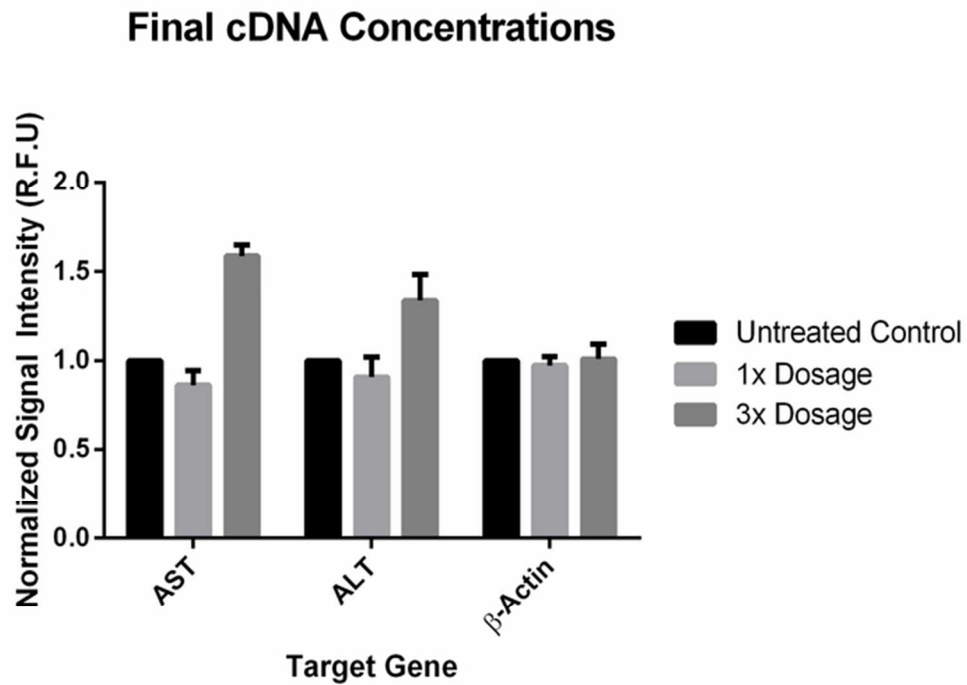
### Final-Primer Concentrations Against Signal Intensities



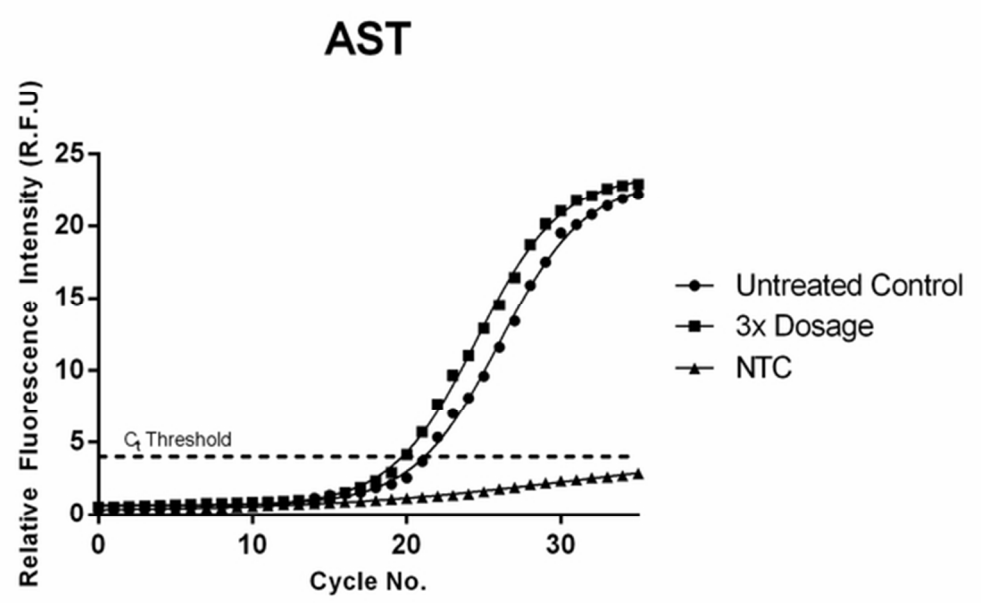
Re-suspension of dried preloaded primers with varying final concentrations in RT-PCR reagent assay for ALT target gene followed by on-chip thermal cycling: a) Gel electrophoresis image showing varying final-primer concentrations (0.1µM, 0.25µM, 0.5µM, 0.75µM and 1.0µM) against a 100bp DNA ladder; b) Signal intensity plot (r.f.u) against final-primer concentration using data derived from gel electrophoresis electropherogram plots. Experiments were performed in triplicates, with error bars shown accordingly.  
54x35mm (300 x 300 DPI)



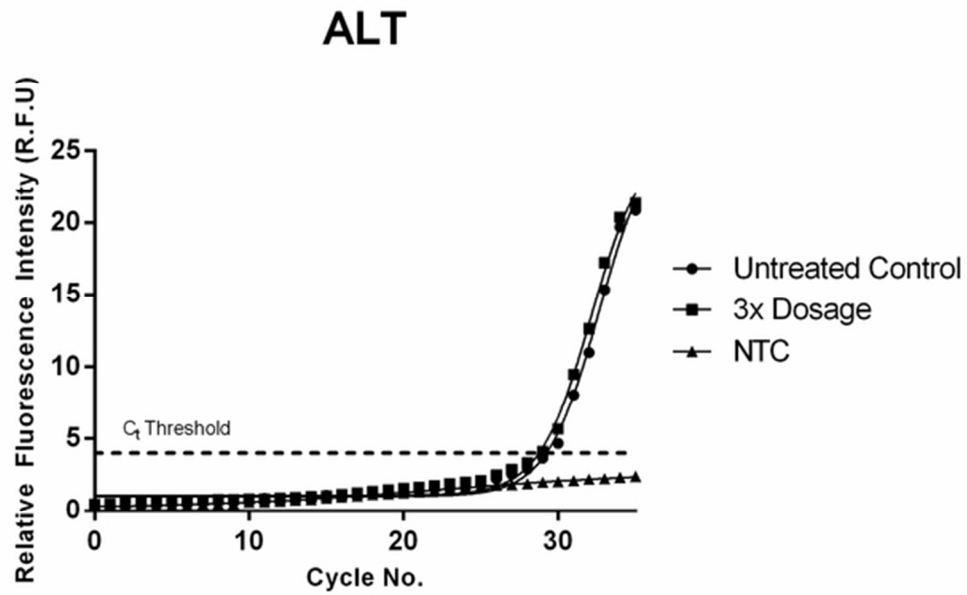
Agarose gel electrophoresis image taken under trans-UV illustrating the specificity of multiplex RT-PCR targeting both ALT and AST genes of interests, and  $\beta$ -actin housekeeping gene from 3x-dosaged mice liver tissue samples. The 12 reaction chambers on our microfluidic chip allowed four replicate groups, each with three target fragments.  
38x17mm (300 x 300 DPI)



Comparison of the differences in AST, ALT and  $\beta$ -actin cDNA concentrations after varying levels (1x and 3x) of drug treatment (cyclophosphamide, 200mg/kg body wt.). Experiments were performed in triplicates, with results normalized to the untreated control.  
60x44mm (300 x 300 DPI)

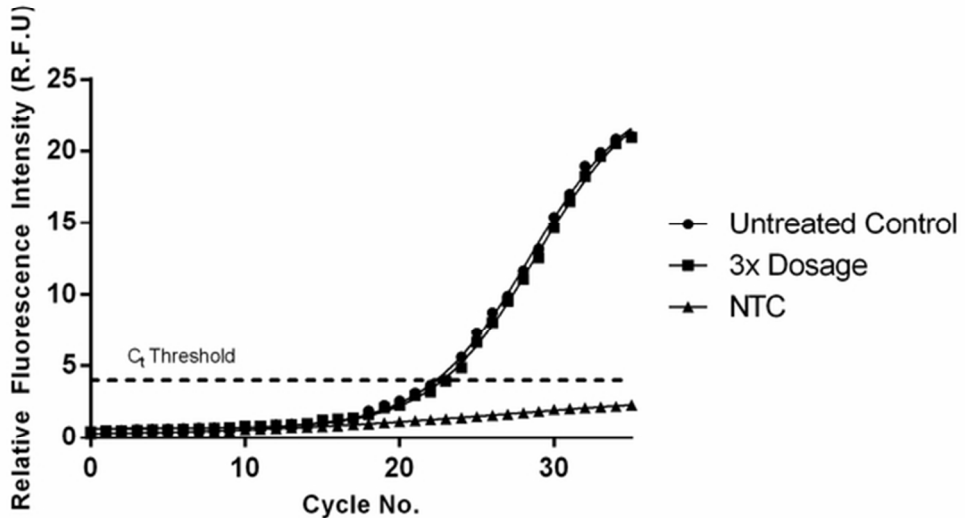


Quantification of real-time fluorescence emission for a) AST, b) ALT and c)  $\beta$ -actin at 3x drug dosage using ImageJ, with images captured at the annealing/extension phase of each PCR cycle.  
52x33mm (300 x 300 DPI)



Quantification of real-time fluorescence emission for a) AST, b) ALT and c)  $\beta$ -actin at 3x drug dosage using ImageJ, with images captured at the annealing/extension phase of each PCR cycle.  
53x34mm (300 x 300 DPI)

### $\beta$ -Actin



Quantification of real-time fluorescence emission for a) AST, b) ALT and c)  $\beta$ -actin at 3x drug dosage using ImageJ, with images captured at the annealing/extension phase of each PCR cycle.  
53x34mm (300 x 300 DPI)

**Table 1** RT-PCR targets and primers sequences (5'-3')

Sequence name	Nucleic acid sequence	Number of base pairs
<i>AST</i> (Target)	GCT GAC TTC TTA GGG CGA TGG TAC AAT GGT ACA GAT AAC AAG AAC ACA CCA ATC TAC GTA TCA TCA CCA ACC TGG GAG AAC CAT AAT GCT GTG TTT TCT GCC GCC GGT TTT AAG GAC ATT CGG CCC TAT TGC TAC TGG GAT GCG GAG AAG AGA GGA CTG GAC CTC CAG GGT TTC CTG AAT GA	182
<i>AST</i> Forward Primer <i>AST</i> Reverse Primer	GCT GAC TTC TTA GGG CGA TG TCA TTC AGG AAA CCC TGG AG	
<i>ALT</i> (Target)	CTG CAG ACC CGA ACA ACA TAT TTC TGT CCA CAG GGG CCA GCG ATG CCA TCG TGA CCA TGC TCA AGC TGC TGG TAG CCG GCG AGG GCC GTG CGC GAA CCG GTG TAC TCA TTC CCA TTC CTC AGT ACC CAC TGT ACT CAG CTG CGC TGG CTG AGC TGG ACG CCG TGC AAG TGG ACT ACT ACC TGA ACG AAG AGC GCG CCT GGG CTC TTG ACA TCG CTG AGC TG	221
<i>ALT</i> Forward Primer <i>ALT</i> Reverse Primer	CTG CAG ACC CGA ACA ACA TA CAG CTC AGC GAT GTC AAG AG	

**Table 2** Comparison of mean  $C_t$  (and corresponding S.D.) values of conventional qPCR machine (CFX96 Touch™) with our microfluidic setup.

<b>No.</b>	<b>mRNA Target</b>	<b>CFX96 Touch™</b>	<b>Microfluidic Chip</b>
<b>1</b>	AST – Control	20.07±0.02	20.5±0.2
<b>2</b>	AST – 3x Dosage	19.34±0.05	19.9±0.2
<b>3</b>	ALT – Control	27.28±0.10	28.8±0.2
<b>4</b>	ALT – 3x Dosage	26.75±0.07	28.5±0.3
<b>5</b>	β-Actin – Control	22.93±0.11	23.0±0.2
<b>6</b>	β-Actin – 3x Dosage	23.02±0.08	23.1±0.2